Comparison of Spectral Estimation Methods in Reconstruction of Parametric Ultrasound Images

Pawan Chaturvedi, Michael F. Insana and Timothy J. Hall

Department of Radiology
University of Kansas Medical Center, Kansas City, KS 66160
email: pawan@research.kumc.edu

ABSTRACT

The application of inverse scattering methods to diagnostic ultrasound echo signals has provided us with detailed information about renal microstructure and function. In particular, the average scatterer size has been used to follow changes in microvascular perfusion that occur early in many renal disease processes. This paper shows that by introducing prior knowledge of the tissue state into the process, uncertainty in the spectral estimate is reduced for low SNR situations, and the contrast and range-resolution in scatterer size images can be improved without increasing the noise. Prior information used in the estimation technique is obtained from the histology of biological tissue. Maximum a posteriori and constrained least squares estimators are designed to obtain images for different levels of noise and for different gate-durations. Prior knowledge about the noise properties and the nature of the echo spectrum is used to obtain the order of an autoregressive model for estimating the power spectral density.

Keywords: spectral estimation, scatterer size imaging, autoregressive, periodogram, maximum a posteriori estimator, constrained least squares estimator.

1 INTRODUCTION

Diagnostic ultrasound imaging has developed into a valuable tool for studying the structure and function of biological tissue. Recent work has shown that the average scatterer size ($\bar{D}$) can be used as a reliable indicator of tissue histology, and the onset of many disease processes has been found to be associated with a change in scattering properties of the tissue[1–5] . Scatterer size images are formed by analyzing the frequency dependence of the echo signal power spectral density (PSD). The PSD is conveniently and efficiently estimated by using a fast Fourier transform (FFT) to obtain an unmodified periodogram[6] .

As with any medical image, the diagnostic utility of scatterer size images depends on their sensitivity to pathology. Sensitivity may be quantified in terms of image contrast, resolution and noise. Due to the often conflicting requirements for these qualities, we usually settle for a trade-off among these properties in an image. For example, when using an unmodified periodogram to estimate scatterer size, the variance in the image can be reduced only at the cost of reduced resolution. Therefore, application-specific techniques that enhance contrast without increasing noise or compromising resolution are desirable.

A simple way of improving the quality of scatterer size images is by incorporating prior information about the problem into the estimation process. Such prior information could consist of the knowledge about the state of the biological tissue, a deterministic model for the target properties, or knowledge of the noise characteristics. In this paper, we investigate how prior knowledge may be used to improve the the low-contrast detectability of scatterer size images.

0-8194-2085-9/96/$6.00

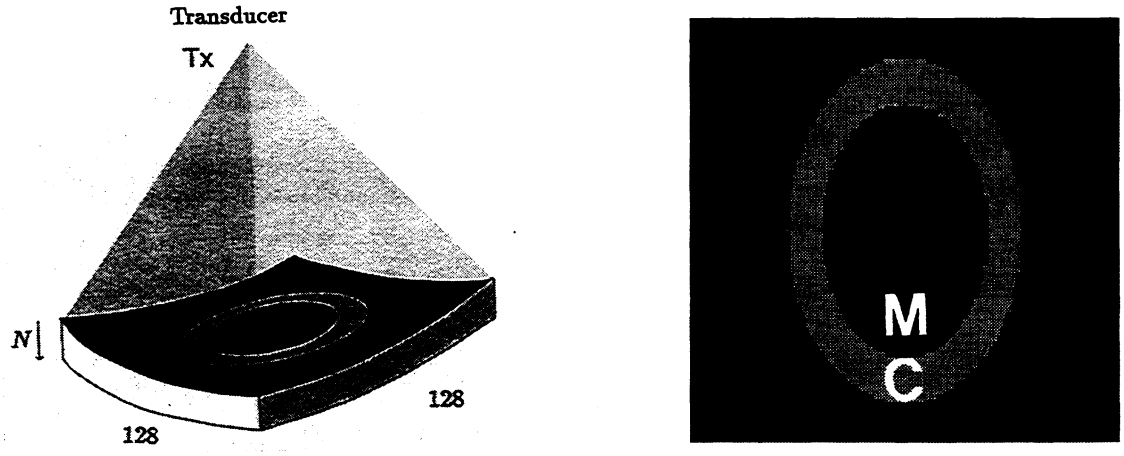

Figure 1: Scanning geometry and the test object used for simulations.

Three different approaches for incorporating prior knowledge into the imaging technique are considered. First, since the echo signal spectra are slowly varying functions of frequency that lack sharp valleys[7] , an autoregressive (AR) model is selected to estimate the PSD in place of the unmodified periodogram[6,8,9] . Knowledge of the noise properties and the nature of the echo spectrum are used for estimating the order of AR model. Second, knowledge about the random structure of the target and the coherent detection process are used to design a maximum a posteriori (MAP) estimator for scatterer size[10–13] . Finally, we discuss the use of prior information about the deterministic properties of the target to design an iterative constrained least squares (CLS) estimator[14,15] for scatterer size. To demonstrate the advantages of incorporating prior knowledge, we compare the results obtained with these estimators against those obtained with a maximum likelihood (ML) estimator using an unmodified periodogram - our current image formation procedure.

In the next section, we briefly describe a model for generating echo signals from a simulated phantom that is used throughout the investigation. The method used for estimating the scatterer size from the return signal is also outlined. In Section 3, AR estimation of the PSD is discussed. A MAP estimator for the acoustic form factor is developed in Section 4, and an iterative CLS approach is presented in Section 5. Several illustrative simulations with these estimators and a discussion of the results are presented in Section 6. Finally, conclusions drawn from this investigation are described in Section 7.

2 ECHO SIGNAL MODEL

A software phantom that simulates acoustic scattering from kidneys in C-scan geometry was used for this investigation as shown in Figure 1. It consists of an outer background region with $\bar{D} = 100\mu$m, an elliptical ring with $\bar{D} = 200\mu$m to simulate the renal cortex, an inner region with $\bar{D} = 50\mu$m to simulate the renal medulla, and a central circular region with $\bar{D} = 75\mu$m. $\bar{D}$ values for the various regions were chosen based on histological observations. Corresponding to each voxel in the 128×128 voxel image, an N-point echo waveform was generated.

The continuous echo signal $x(t)$ is obtained by convolving the tissue response $r(t)$ with the system point spread function $h(t)$ that accounts for properties of the transducer and the intervening medium. Adding noise and transforming to the Fourier domain yields

$$X(k) = H(k)R(k) + N(k), \tag{1}$$

where $k = 2\pi f/c$ is the spatial frequency variable, f is the temporal frequency variable, and c is the speed of sound. For simplicity, we assume that N is uncorrelated white Gaussian noise with zero mean as indicated by the notation $\mathcal{N}(0, \sigma_n^2)$. Although the relationship between the parameter estimated $\bar{D}$ and the echo data X is nonlinear, we can linearize the problem by estimating the tissue response function R, and then computing $\bar{D}$ from R. For acoustic scattering by the kidney, the tissue response can be accurately modeled by a function[4,5] of the form $R = k^2 \exp\{-k^2\bar{D}^2/3.11^2\}$. The form factor defined as $F(k) = R^2(k)$ is more commonly used to describe the acoustical scattering properties of biological tissue. Using a simplified model for the system response, $h(t)$ can be modeled as a product of a sinusoid with a Gaussian pulse:

$$H(k) = \frac{j}{2}\left[\exp\left\{-(k+k_0)^2\sigma^2/2\right\} - \exp\left\{-(k-k_0)^2\sigma^2/2\right\}\right], \tag{2}$$

where k_0 is the center frequency of the transducer and σ determines the width of the pulse. Eqs. (1) and (2) were used for generating echo waveforms by taking the inverse Fourier transform to obtain the time-varying signals.

The tissue response R can be used to completely identify the effects of scatterer size on the echo signal. All other terms are factored out from the return signal after performing a Fourier transform. R thus obtained is compared against the theoretically computed tissue response for several scatterer sizes. A mean squared error criterion is used for comparison, and the estimate $\hat{D}$ that results in the minimum error is assigned to the corresponding voxel in the image.

3 AUTOREGRESSIVE (AR) SPECTRAL ESTIMATION

As mentioned previously, scatterer size estimates can be formed by extracting the form factor from the PSD of the signal. The standard method for estimating the PSD is an unmodified periodogram, which is obtained by directly taking the magnitude squared of the Fourier transform of the signal:

$$\hat{P}_{xx}^{P}(k) = \frac{1}{T}|X(k)|^2, \tag{3}$$

where T is the inter-sample period. However, since we also know from earlier work that the echo spectrum contains no sharp valleys, we can use an AR model to estimate the PSD. In an AR model, the discrete echo-signal is represented as an all-pole waveform of appropriate order,

$$x[n] = -\sum_{k=1}^{p} a[k]x[n-k] + u[n], \tag{4}$$

where $u[n]$ is a zero-mean white Gaussian noise process with variance ρ_w, $a[k]$ are the AR coefficients, and p is the order of the AR model. Using this representation, the signal is completely identified by the AR coefficients. If a smooth signal is desired, a low order AR model is used, and for rapidly varying signals, an AR model of high order can be used. Several algorithms exist for determining the order of the model when the signal is known to be truly AR. Since that is not generally true for echo waveforms from biological tissue, we estimate the approximate order from knowledge of the noise properties and the smooth Gaussian nature of the underlying process. Once the order of the model has been established, one of several available algorithms can be used to determine the AR coefficients $a[k]$. We use Burg's algorithm for this work.

From the AR coefficients, the PSD can be obtained by using the following relationship:

$$\hat{P}_{xx}^{AR}(f) = \frac{T\rho_w}{|A(f)|^2}, \tag{5}$$

where $A(f)$ is the Fourier transform of the AR coefficients as given by

$$A(f) = 1 + \sum_{k=1}^{p} a[k] \exp\{-i2\pi f k T\}. \tag{6}$$

Scatterer size is determined using the ML estimate, with the PSD P_{xx} computed from periodogram or AR technique related to $\bar{D}$ by

$$P_{xx}(k) = k^4 |H(k)|^2 \exp\{-2k^2\bar{D}^2/3.11^2\}. \tag{7}$$

4 MAXIMUM A POSTERIORI (MAP) ESTIMATION

Bayesian analysis provides a powerful estimation technique for constructing images of stochastic objects when knowledge about the distribution of the object is available. For example, MAP estimates improve the results by conditioning the solution to the inverse problem based on this information. MAP estimates converge to ML estimates when no prior information is available[11,13] . The basis for estimation is provided by the Bayes' theorem for conditional probability. Depending on whether the mean, median or the mode of the pdf is used, different type of estimators can be designed. The MAP estimator maximizes the mode of the posterior probability density function (pdf), $\mathrm{p}(R|X)$.

To develop an estimate for R, we recall from Bayes' theorem that

$$\mathrm{p}(R|X) = \frac{\mathrm{p}(X|R)\mathrm{p}(R)}{\mathrm{p}(X)}. \tag{8}$$

In Eq. (1), $\mathrm{p}(X)$ is the pdf of the data which is assumed to be independent of the object function. $\mathrm{p}(X|R)$ denotes the distribution of the data given a tissue response function, and is called the likelihood of X. $\mathrm{p}(R)$ represents the knowledge about the distribution of R before the measurements were taken, and is known as the prior. $\mathrm{p}(R|X)$ is the distribution of R obtained by updating the prior with the measurements, and is known as the posterior probability.

For uncorrelated white Gaussian noise used in the signal model given by Eq. (1), the likelihood is Gaussian $\mathcal{N}(\langle HR\rangle, \sigma_n^2)$, with $\langle . \rangle$ defining the average over all noise $N(k)$ for a given $R(k)$. Moreover, we assume in our model that the object function R is Gaussian $\mathcal{N}(\bar{R}, \sigma_r^2)$. Note that while σ_n^2 is a constant because the noise spectrum is white, $\sigma_r^2(k)$ is a function of frequency since the object spectrum is not white. Using this knowledge in Eq. (8), the MAP estimate is obtained by maximizing the negative logarithm of the posterior probability:

$$-\log \mathrm{p}(R|X) = \frac{1}{2\sigma_n^2}(X - HR)^*(X - HR) + \frac{1}{2\sigma_r^2}(R - \bar{R})^2 + \log \mathrm{p}(X), \tag{9}$$

where $*$ denotes the complex conjugate of the quantity and $\bar{R}$ is the mode (which is same as the mean for a Gaussian distribution) of the object function R. To maximize Eq. (9), we recall that R is real and even, whereas H is imaginary and odd. Using these properties and setting the derivative of Eq. (9) to zero,

$$-\frac{1}{\sigma_n^2}H^*X + \frac{1}{\sigma_n^2}H^*HR + \frac{1}{\sigma_r^2}(R - \bar{R}) = 0. \tag{10}$$

Simplifying and rearranging the terms in Eq. (10), we obtain the MAP estimate of R as:

$$\hat{R}_{MAP} = \frac{H^*X + \gamma_{MAP}\bar{R}}{H^*H + \gamma_{MAP}}. \tag{11}$$

where $\gamma_{MAP} = \sigma_n^2/\sigma_r^2(k)$. The prior information is incorporated into the solution through $\bar{R}$. The MAP estimator puts more or less weight on the prior depending on the noise level relative to the object variability. When the SNR for the echo signals is high, the solution is primarily determined from the data. Otherwise, more weight is assigned to the prior knowledge. The ML estimate is obtained by substituting $\gamma_{MAP} = 0$ into Eq. (11), indicating lack of any reliable prior information.

5 ITERATIVE CONSTRAINED LEAST SQUARES (CLS) ESTIMATION

A least squares solution minimizes the norm of the error for a deterministic problem. Because of its simplicity and effectiveness for a wide class of problems, it is extensively used in imaging applications. However, many practical problems are ill-posed, and, for such cases, the least squares approach results in an unstable solution. However, by applying appropriate constraints based on prior information, the solution can be improved and the ill conditioning of the problem can be alleviated[15] . We develop a CLS estimate for R in this section.

Whereas the least squares solution is obtained simply by minimizing the norm of error between the model and the data, the CLS estimate can be derived by constraining the solution based on prior knowledge about the object function. Therefore, to obtain the CLS solution, we minimize the functional:

$$f(R) = \|X - HR\|^2 + \gamma_{CLS}\|R - \bar{R}\|^2, \tag{12}$$

where γ_{CLS} is the Lagrangian multiplier that determines the weight assigned to the constraint. As in case of γ_{MAP}, the most appropriate value for γ_{CLS} depends on the noise in the echo data. The prior knowledge about the object function determines $\bar{R}$. Taking the derivative of $f(R)$ with respect to R and setting the result to zero:

$$-H^*X + \gamma_{CLS}H^*HR + \gamma_{CLS}(R - \bar{R}) = 0. \tag{13}$$

On simplification, Eq. (13) yields the CLS estimator as

$$\hat{R}_{CLS} = \frac{H^*X + \gamma_{CLS}\bar{R}}{H^*H + \gamma_{CLS}}. \tag{14}$$

A comparison of Eqs. (11) and (14) indicates that the mathematical forms of the two estimators are identical except for the physical interpretation of the weights assigned to the prior. While the expression for γ_{MAP} follows naturally from knowledge of the statistics of the object function and the noise, γ_{CLS} must be determined in a separate inverse problem or estimated empirically. Due to the high overhead involved in the computation of γ_{CLS}, the empirical approach is frequently used to determine an optimal value.

The CLS approach provides a convenient method of incorporating prior knowledge into the solution to improve the quality of the image. A one-step approach as outlined above is often insufficient when the data quality is poor or the prior knowledge is imprecise. In such cases, multiple iterations of the CLS estimate improve the quality of results. At successive iterations, the prior estimate is improved by using the image obtained at the previous iteration as the prior estimate. Therefore, the iterative scheme can be represented as:

$$\hat{R}^{\ell+1}_{CLS} = \frac{H^*X + \gamma^{\ell}_{CLS}\hat{R}^{\ell}_{CLS}}{H^*H + \gamma^{\ell}_{CLS}}. \tag{15}$$

Gradual introduction of the data into the solution instead of finding an optimal estimate with one iteration significantly improves image quality for low SNR measurements as will be shown in the next section.

6 RESULTS AND DISCUSSION

Echo signals were generated according to the model described in Section 2, and several simulations were performed to study the effect of using different estimators. A center frequency of 5 MHz and a sampling rate of 25 MHz were selected. Performance of the estimators was investigated both as a function of the echo waveform

SNR and gate duration. The latter study is important in determining the utility of the approach for high-resolution imaging of thin slices of tissue. For high SNRs, a nominal frequency bandwidth of 60% of the center frequency was used, and for low SNR studies, 40% bandwidth was used for imaging. A contrast-to-noise ratio (CNR) was defined to quantify the quality of image reconstruction:

$$\mathrm{CNR} = \frac{(\bar{D}_i - \bar{D}_j)^2}{\mathrm{var}D_i + \mathrm{var}D_j}, \tag{16}$$

where i and j represent two adjacent regions in the test object. For this work, the CNR between the simulated cortex and medulla regions was used as the indicator of image quality.

Reconstruction of the test object shown in Fig. 1 using an unmodified periodogram is depicted in Fig. 2a when a 256-point echo signal at 20 dB SNR is used. An ML estimator was employed to obtain the tissue response R from the PSD. The corresponding images with the AR and a single iteration of the CLS approach (which was forced to be identical to the MAP estimate by choosing $\gamma_{CLS} = \gamma_{MAP}$) are shown in Fig. 2b and c, respectively. Based on the fact that the noise level is lowest near the center of the measurement bandwidth and increases towards the edges of the bandwidth according to the shape of the pulse, $\gamma_{CLS}(k) = \mathrm{const}/|H(k)|^2$ was chosen for this work, with the constant of proportionality determined empirically from the data. Using this expression for γ_{CLS} resulted in more weight being place on the measurements near the center frequency of the transducer.

Due to the long duration of the signal, the effects of windowing on the PSD are not significant when the PSD is estimated using an unmodified periodogram. However, even for this simulation, use of AR or CLS technique clearly results in a better image. Since the noise level is low, a high order AR model can be used to improve the resolution in the image. The image shown in Fig. 2b was obtained with an eighth order AR model. While the CLS estimator resulted in a higher CNR as shown in Table 1, the bias was lower in the image obtained with the AR technique. The prior $\bar{R}$ used in Eq. 14 consisted of a uniform image with a scatterer size $\bar{D} = 100\mu$m. Therefore, this prior information constrained the solution to be smooth.

Images of the test object for data at 5 dB SNR are shown in Fig. 2d-f. The effect of noise on the image obtained with the unmodified periodogram can be easily seen, and the improvement in images obtained on using the prior knowledge becomes more apparent for this case. Due to the high level of noise, a fifth order AR model was used to suppress the rapid fluctuations in the spectrum since it is known that the spectrum of the signal itself is fairly smooth. Moreover, unlike for the previous case in which a single iteration of CLS technique was sufficient, use of multiple iterations resulted in a significant improvement in image quality. The result shown in Fig. 2f was obtained with three iterations.

A study of the variation of CNR with γ_{CLS} provides interesting physical insight into the reconstruction process. For a 256-point segment at 5 dB SNR, the variation of CNR is shown in Fig. 3 for one, two and three iterations. For multiple iterations, a slightly higher than optimal value was chosen for the first (and second) iteration to obtain a smooth estimate which is then used as the prior in subsequent iterations. The plots clearly show the nonlinear nature of the curve and illustrate how multiple iterations yield a CNR that is almost twice as high as the one obtained with a single iteration. $\gamma_{CLS} = 0$ corresponds to the ML solution, and $\gamma_{CLS} = \infty$ corresponds to the perfectly smooth prior estimate with zero contrast.

A similar set of simulations was performed with 32-point echo waveforms. The information content was proportionately lower for this case. For an SNR of 20 dB, the reconstructions with the periodogram, AR and two iterations of the CLS technique are shown in Fig. 4a, b and c, respectively. The effect of small gate-duration is clearly apparent in the image obtained with the periodogram estimate, and various regions of the test object are barely visible. However, use of AR or CLS estimate dramatically improves the quality of the reconstruction. Knowledge about the noise properties and the tissue state was again used to choose the correct order of the AR model and the value of γ_{CLS}. These simulations indicate that by using prior information, we can obtain high-quality images of thin tissue slices when conventional processing techniques perform poorly. Even in the presence of high levels of noise, the outlines of various regions in the image can still be seen as shown in Fig. 4e-f for 5 dB SNR, although the reconstruction is not as impressive with the CLS method as it is with the AR

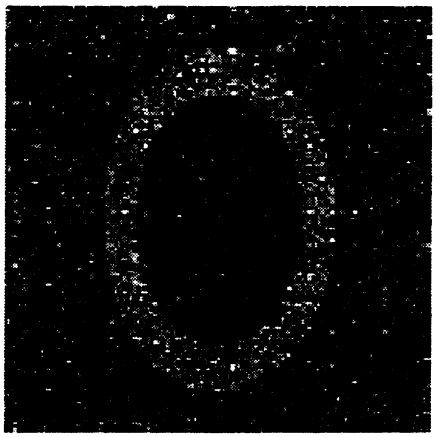

(a) ML estimate with periodogram

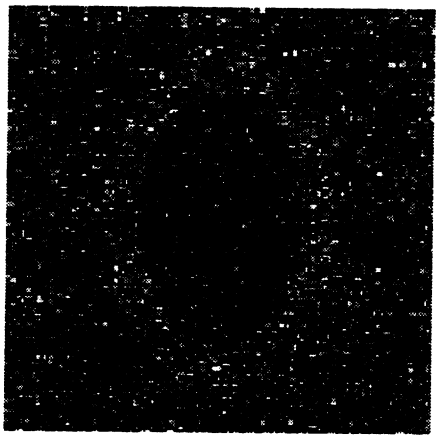

(d) ML estimate with periodogram

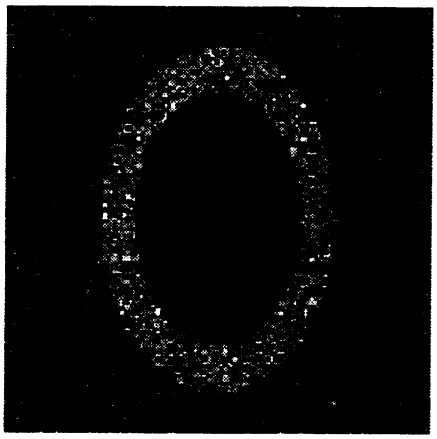

(b) ML estimate with AR model

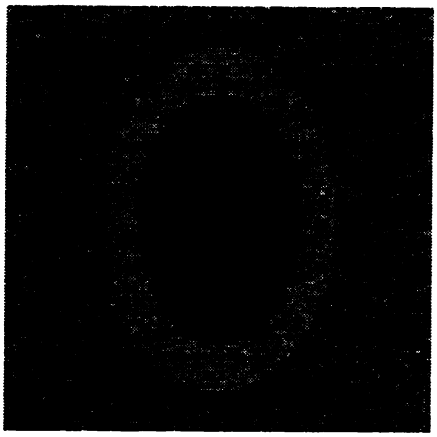

(e) ML estimate with AR model

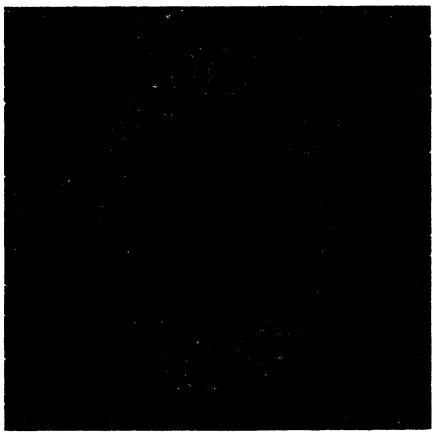

(c) CLS estimate

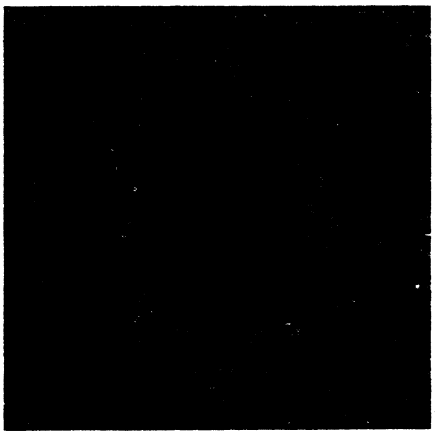

(f) CLS estimate

Figure 2: Images obtained with a 256-point signal (10.2 mm slice thickness). (a)-(c) were obtained with 20 dB SNR and (d)-(f) with 5 dB SNR.

N	SNR	Technique	CNR×100	$\bar{D}_{medulla}$	$\bar{D}_{cortex}$
256	20 dB	ML-Periodogram	314.48	61.31	206.08
		ML-AR	755.56	49.49	199.75
		CLS/MAP	2721.07	15.75	102.86
	5 dB	ML-Periodogram	86.87	92.49	183.64
		ML-AR	630.68	64.31	186.33
		CLS	254.95	22.42	93.03
32	20 dB	ML-Periodogram	51.16	83.80	181.19
		ML-AR	464.35	38.52	167.96
		CLS	245.67	31.16	144.40
	5 dB	ML-Periodogram	1.01	130.71	148.33
		ML-AR	95.33	84.48	137.66
		CLS	9.47	63.08	105.42

Table 1: CNR and $\bar{D}$ for medulla and cortex regions for various simulations (C and M in Fig. 1).

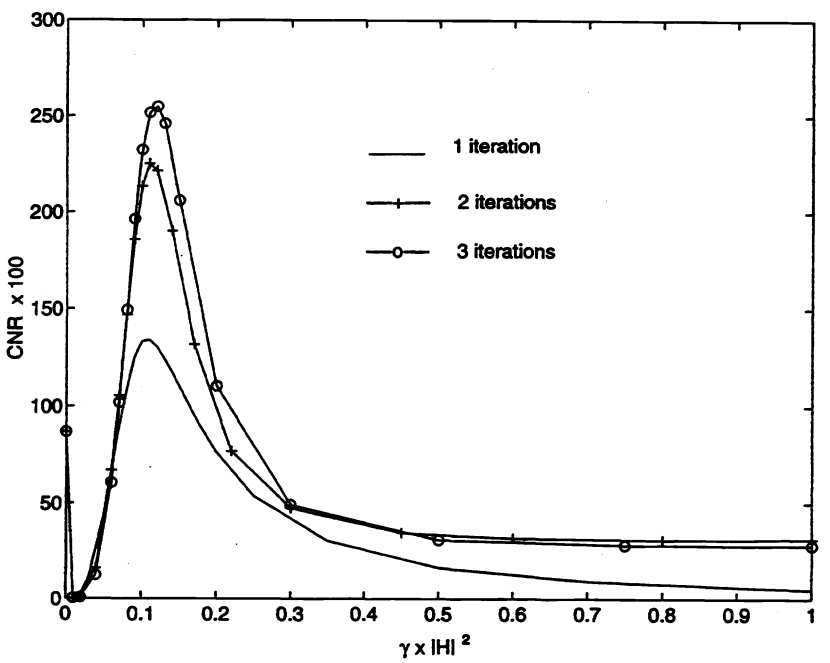

Figure 3: Contrast-to-noise ratio (CNR) obtained with iterative CLS technique for a 256-point segment at 5 dB SNR. Solid line: 1 iteration; –+–: 2 iterations; –o–: 3 iterations.

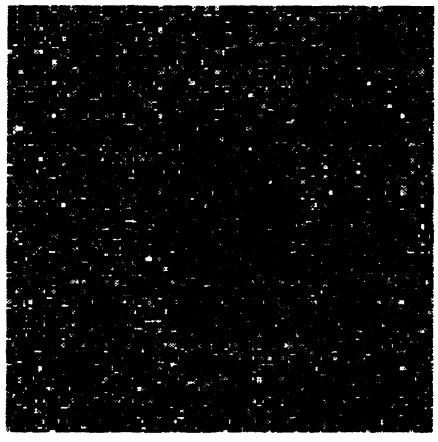

(a) ML estimate with periodogram

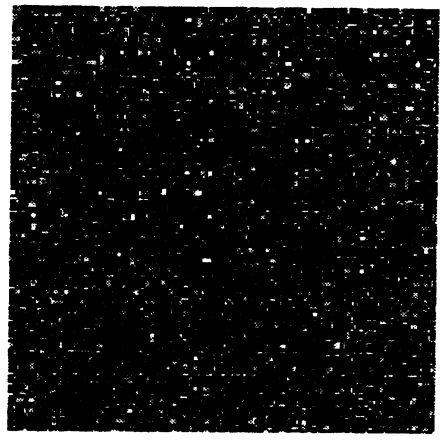

(d) ML estimate with periodogram

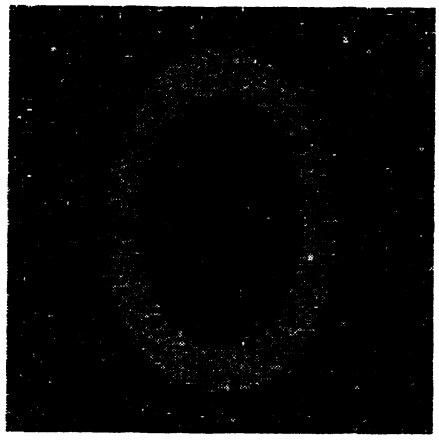

(b) ML estimate with AR model

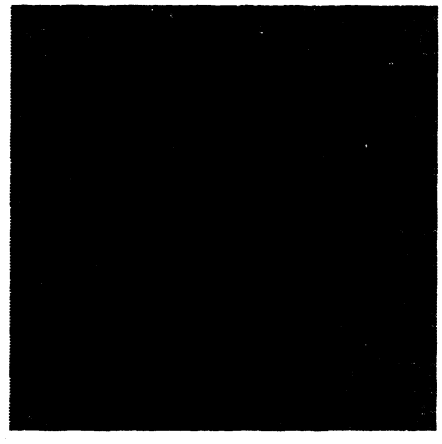

(e) ML estimate with AR model

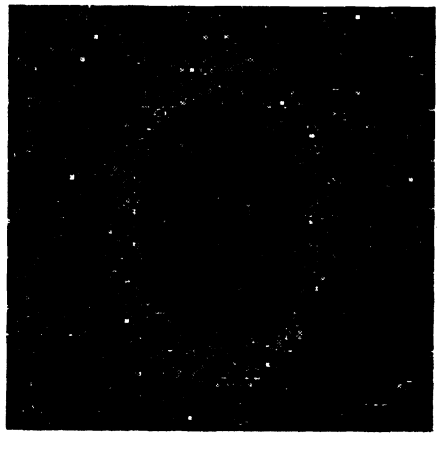

(c) CLS estimate

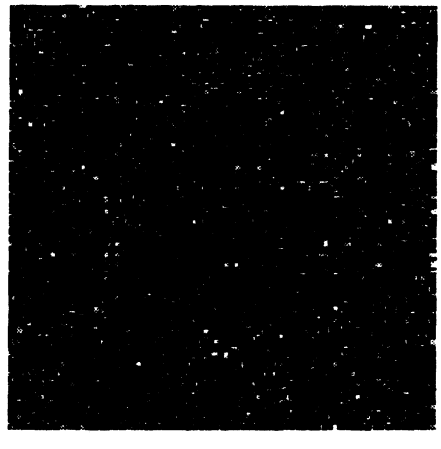

(f) CLS estimate

Figure 4: Images obtained with a 32-point signal (1.28 mm slice thickness). (a)-(c) were obtained with 20 dB SNR and (d)-(f) with 5 dB SNR.

technique. Features of the target are completely masked by noise and artifacts induced by the short range gate for this case when an unmodified periodogram is used. The corresponding image is shown in Fig. 4d.

In many of the simulations, the central circular region with $\bar{D} = 75\mu$m is completely lost in the image. The lack of contrast in this region is more a consequence of the center frequency of the transducer than a limitation of the imaging technique itself[4] . At a center frequency of 5 MHz, the echo spectrum is most sensitive to changes near $\bar{D} \approx 100\mu$m (since $ka \approx 1$ for $\bar{D} = 100\mu$m). Therefore, regions with $\bar{D} = 75$ and 50μm are not seen as separate regions. When a similar investigation was performed at a higher operating frequency, the central region was easily visible. To illustrate this effect, the ML reconstruction of the same test object for a 256-point echo signal at 20 dB SNR, using a center frequency of 8 MHz and a nominal bandwidth of 60%, is shown in Fig. 5. While the central region is clearly seen in this image, the cortical region in the reconstruction is significantly degraded since $ka \approx 3.3$ in that region.

In addition to the increased computation time, the AR ML estimate and the iterative CLS technique decrease the variance in the image often at the cost of increased bias. However, the process results in a net increase in the CNR as shown in Table 1. Despite the introduction of bias in the estimates, the drastic increase in CNR achieved when prior information is used provides a distinct advantage for medical imaging.

7 CONCLUSIONS

Prior knowledge about the nature of echo signals and noise characteristics can be used to improve the contrast and suppress noise in scatterer size images. Use of prior information is particularly useful when the noise level is high and/or the signal duration (C-scan slice thickness) is small. High range-resolution is achieved by using imaging techniques that use such information. Robustness and resolution capabilities of these estimators can be potentially very useful in clinical applications. The improved CNR and resolution in the images is at the cost of a larger bias in the estimates and increased computation time.

8 REFERENCES

[1] Silverman, R.H., Coleman, D.J., Lizzi, F.L., Torpey, J.H., Driller, J., Iwamoto, T., Burgess, S.E., and Rosado, A., "Ultrasonic tissue characterization and histopathology in tumor xenografts following ultrasonically induced hyperthermia," *Ultrasound Med. Biol.*, vol. 12, pp. 639-645, 1986.

[2] Lizzi, F.L., Ostromogilsky, M., Feleppa, E.J., Rorke, M.C., and Yaremko, M.M., "Relationship of ultrasonic spectral parameters to features of tissue microstructure," *IEEE Trans. Ultrason., Ferroelect., Freq. Contrl.*, vol. 34, pp. 319-329, 1987.

[3] Chandrasekaran, K., Aylward, P.E., Fleagle, S.R., Burns, T.L., Seward, J.B., Tajik, A.J., Collins, S.M., and Skorton, D.J., "Feasibility of identifying amyloid and hypertrophic cardiomyopathy with the use of computerized quantitative texture analysis of clinical echocardiographic data," *J. Am. Coll. Cardiol.*, vol. 13, pp. 832-840, 1989.

[4] Insana, M.F. and Hall, T.J., "Parametric ultrasound imaging from backscatter coefficient measurements: image formation and interpretation," *Ultrasonic Imaging*, vol. 12, pp. 245-267, 1990.

[5] Insana, M.F., Hall, T.J., Wood, J.G., and Yan, Z.Y., "Renal ultrasound using parametric imaging techniques to detect changes in microstructure and function," *Invest. Radiol.*,vol. 28, pp. 720-725, 1993.

[6] Marple, S.L., *Digital Spectral Analysis With Applications*, Prentice Hall, Englewood Cliffs NJ, 1987.

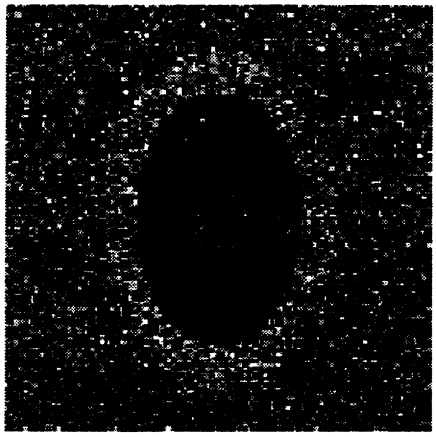

Figure 5: ML reconstruction of the test object for a 256-point echo signal at 20 dB SNR when the transducer center frequency is 8 MHz and nominal bandwidth is 60%.

[7] Wagner, R.F., Insana, M.F., and Brown, D.G., "Statistical properties of radio-frequency and envelope detected signals with applications to medical ultrasound," *J. Opt. Soc. Am. A 4*, 910-922 (1987).

[8] Wear, K.A., Wagner, R.F., and Garra, B.S., "High resolution ultrasonic backscatter coefficient estimation based on autoregressive spectral estimation," *IEEE Trans. Med. Imag.*, vol. 13, pp. 500-507, 1994.

[9] Wear, K.A., Wagner, R.F., and Garra, B.S., "A comparison of autoregressive spectral estimation algorithms and order determination methods in ultrasonic tissue characterization," *IEEE Trans. Ultrason., Ferroelect., Freq. Contrl.*, vol. 24, pp. 709-716, 1995.

[10] Hunt, B.R., "Bayesian methods in nonlinear digital image restoration," *IEEE Trans. Computers*, vol. C-26, pp. 219-229, 1977.

[11] Hanson, K.M., "Bayesian and related methods in image reconstruction from incomplete data," in *Image Recovery: Theory and Application*, ed. H. Stark, Academic Press, Orlando, pp. 79-125, 1987.

[12] Geman, S., and Geman, D., "Stochastic relaxation, Gibb's distributions, and Bayesian restoration of images," *IEEE Trans. Pattern Anal. Machine Intell.*, vol. PAMI-6, pp. 721-741, 1984.

[13] Hanson, K.M., "Reconstruction based on flexible prior models," *Proc. SPIE*, vol. 1652, pp. 183-191, 1992.

[14] Twomey, S., *Introduction to the Mathematics of of Inversion in Remote Sensing and Indirect Measurements*, Elsevier Scientific Publishing, New York, 1977.

[15] Gonzalez, R.C., and Wintz, P., *Digital Image Processing*, 2nd. ed., Addison-Wesley, Reading, MA, 1987.